Sliding-Mode MRAS Speed Estimators for Sensorless Vector Control of Induction Machine

Mihai Comanescu, *Student Member, IEEE*, and Longya Xu, *Fellow, IEEE*

***Abstract*—This paper presents two novel sliding mode (SM) model reference adaptive system (MRAS) observers for speed estimation in a sensorless-vector-controlled induction-machine drive. Both methods use the flux estimated by the voltage model observer as the reference and construct SM flux observers that allow speed estimation. Stability and dynamics of the two proposed SM flux observers are discussed. The observers are compared with the classical MRAS observer. The proposed estimators seem very robust and easy to tune. Unlike the classical MRAS, the speed-estimation process is based on algebraic calculations that do not exhibit underdamped poles or zeros on the right-hand plane. Simulations and experimental results on a 1/4-hp three-phase induction machine confirm the validity of the approaches.**

***Index Terms*—Induction machine, model reference adaptive system (MRAS), sensorless control, sliding-mode (SM) observers, speed estimation, vector control.**

I. Introduction

SEVERAL methods are available for rotor speed estimation in a sensorless induction-machine drive and they have been extensively studied in the last few decades. The speed estimate is mandatory if speed control (feedback) is employed. Also, the speed estimate is needed if decoupling is intended in the current regulation loops of the rotational reference frame.

In a sensorless induction-machine drive, the speed can be estimated by various techniques [1]. A speed estimate can be directly obtained using the machine's model equations; however, the accuracy is not very good. Speed estimation based on the slip equation is quite popular and simple to implement. Other techniques are also available: the extended Kalman filter method and the Luenberger observer construct full-order estimators based on the machine model. Both approaches tend to depend heavily on the machine parameters and are generally difficult to implement. Lately, sliding mode (SM) observers have been reported for the estimation of the variables of interest of the induction machine (rotor fluxes, speed, and rotor time constant). Another viable solution for speed estimation is the model reference adaptive system (MRAS) method.

The main concerns regarding speed estimation are related to steady-state accuracy, dependence on motor parameters, estimation bandwidth, and dynamic behavior. An additional problem that occurs in implementation is the ripple-versus-delay tradeoff. Very often, the speed estimate requires low-pass filtering and the delay introduced by filters reduces the system's phase margin and can cause instability.

The classical rotor flux MRAS method was first reported in [2]; it is also treated in [3]–[5]. The approach is based on parameter adaptation in a speed-dependent flux observer such that the observer's outputs match a speed-independent reference model. The back electromotive force (EMF) MRAS method [6] is constructed on the same principle but uses the stationary-frame EMF components as reference.

In this paper, we first analyze the behavior, estimation dynamics, and selection of the controller parameters for the classical rotor-flux MRAS method under ideal and nonideal integration. The back EMF MRAS is believed to have inferior performance [4], [5] and will not be discussed.

Later, we propose two MRAS speed-estimation methods that are based on SM observers for the adjustable model and we compare their behavior with the classical MRAS. Finally, we present simulations and experimental results on a 1/4-hp three-phase induction machine to validate the proposed speed-estimation methods.

II. Dynamics of Classical MRAS

The rotor-flux MRAS method presented in [2] uses the voltage model (VM) as the reference and the current model (CM) as adjustable model to estimate the motor speed.

The VM computes the stator and rotor fluxes in the stationary reference frame as

$$\lambda_{\rm s} = \int (V_{\rm s} - R_{\rm s} I_{\rm s}) dt = \int e_{\rm s} dt \tag{1}$$

$$\lambda_{\alpha\beta}^{\rm ref} = \frac{L_{\rm r}}{L_{\rm m}} (\lambda_{\rm s} - L_{\rm s} \sigma I_{\rm s}) \tag{2}$$

where $\lambda_{\rm s}$, $\lambda_{\alpha\beta}^{\rm ref}$ are the stator and rotor-flux vectors.

Equations of the CM observer are

$$\frac{d\hat{\lambda}_\alpha}{dt} = -\eta \hat{\lambda}_\alpha - \hat{\omega}_{\rm r} \hat{\lambda}_\beta + \eta L_{\rm m} I_\alpha \tag{3}$$

$$\frac{d\hat{\lambda}_\beta}{dt} = \hat{\omega}_{\rm r} \hat{\lambda}_\alpha - \eta \hat{\lambda}_\beta + \eta L_{\rm m} I_\beta. \tag{4}$$

The speed estimate is then obtained by feeding the error term ε given by (5) into a PI controller.

$$\varepsilon = \lambda_\beta^{\rm ref} \hat{\lambda}_\alpha - \lambda_\alpha^{\rm ref} \hat{\lambda}_\beta. \tag{5}$$

A block diagram of the classical rotor-flux MRAS method is shown in Fig. 1.

Manuscript received May 8, 2004; revised September 9, 2004. Abstract published on the Internet November 25, 2005.

M. Comanescu was with the Department of Electrical and Computer Engineering, The Ohio State University, Columbus, OH 43210 USA. He is now with Azure Dynamics, Woburn, MA 01801-2103 USA.

L. Xu is with the Department of Electrical and Computer Engineering, The Ohio State University, Columbus, OH 43210 USA (e-mail: xu.12@osu.edu).

Digital Object Identifier 10.1109/TIE.2005.862303

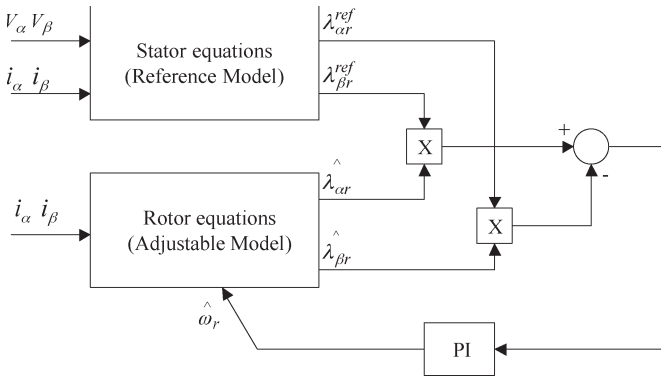

Fig. 1. Block diagram of classical rotor-flux MRAS method.

The performance and the dynamics of the MRAS speed estimator were studied in [2]. If ideal integration is used in both the reference and the adjustable model, the transfer function from the change in speed $(\Delta\omega_{\rm r})$ to the change in estimated speed $(\Delta\hat{\omega}_{\rm r})$ is of the third order (Fig. 2) and $G_1(s)$ is given by (6). The slip frequency, inverse of the rotor time constant, and flux magnitude are denoted as $\omega_{\rm sl}$, η, and λ_0

$$G_1(s) = \frac{(s+\eta)}{(s+\eta)^2 + \omega_{\rm sl}^2}. \tag{6}$$

The root locus of the speed-estimation process in Fig. 2 shows that gains K_p and K_i can be selected to obtain two critically or overdamped poles. The third pole cannot be made faster than $-\eta$. The performance of the speed estimation obtained in such a way is limited but the dynamics may still be acceptable.

In [3], the simplifying assumption $\omega_{\rm sl} = 0$ is made and algebraic expressions for the PI gains are obtained as a function of the desired poles. Indeed, in this case, the factor $(s+\eta)$ can be simplified from the expression of $G_1(s)$ and the closed-loop transfer function obtained is of the second order. Despite the assumption (most likely not true), our simulation study suggests that this method is very useful for selecting the PI gains. The estimation results following the approach in [3] and those by the third-order system in Fig. 2 behave nearly the same.

Generally, the classical MRAS works very well if ideal integration can be used in both models: The fluxes of the adjustable model converge to the reference fluxes and the speed estimate has small or no steady-state error. Also, the dynamics of the speed estimate is acceptable.

However, in a real system, pure integration cannot be implemented for various reasons. Several alternative methods are already available, [7], [8]; generally, they are difficult to implement on 16-bit fixed-point processors. To overcome the problems due to offsets in the voltage/current signals or due to nonzero-flux initial conditions, low-pass filters (LPFs) are used instead of integrators in both the reference and the adjustable models. In this paper, the LPF technique will be referred to as "nonideal integration."

When LPFs are used in the classical MRAS, the model in Fig. 2 is augmented and right-hand-plane zeros appear in the speed-estimation loop. The effect of the right-side zeros is not acceptable: When a change in the real speed occurs, the speed estimate changes in the opposite direction during the initial transient. In a sensorless-vector-controlled drive, this can lead to oscillations or cause a disproportionate response of the speed controller. The introduction of high-pass filters as in [2] and [3] to compensate the effect of nonideal integration may not change this behavior. Additional problems occur if high PI gains are designed—under noise conditions, they must be reduced and an underdamped response is obtained.

Simulation results of the classical MRAS are shown in Figs. 3 and 4, and these will be later compared with our proposed speed-estimation techniques. The PI gains of the MRAS estimator have been designed using the approach in [3] for critically damped poles; the values are $K_p = 674.5$, $K_i = 24\,649$. LPFs with 3.18-Hz cutoff frequency are used in both the VM and CM observers to avoid ideal integration. The flux magnitude is $\lambda_0 = 0.4$ Wb, $\eta = 17.68$, $T_{\rm load} = 0.2$ pu.

Initially, the motor is started to run at 500 r/min. At $t = 0.3$, the reference speed is changed to 750 r/min and Fig. 3 shows the dynamics of the speed estimate versus the real speed. As expected, the right-hand side zeros in the speed-estimation loop cause a dip in the speed estimate at $t = 0.3$ s.

Also, under nonideal integration, the fluxes estimated by the adjustable model deviate substantially from the references (Fig. 4).

Fig. 5 shows the experimental waveform of the speed estimate for a 500–700-r/min acceleration using the classical MRAS method that confirms the computer-simulation results. Fig. 6 shows the reference and observed α fluxes under nonideal integration at a speed of approximately 500 r/min. Note that the magnitudes are different and they correspond to the simulation.

III. MRAS Single-Manifold SM Observer

For the speed-estimation method proposed below, the rotor fluxes $\lambda_\alpha^{\rm ref}$ and $\lambda_\beta^{\rm ref}$ are obtained by the VM observer and they also satisfy the rotor equations. Thus, (7) and (8) are obtained as follows:

$$\frac{d\lambda_\alpha^{\rm ref}}{dt} = -\eta\lambda_\alpha^{\rm ref} - \omega_{\rm r}\lambda_\beta^{\rm ref} + \eta L_{\rm m} I_\alpha \tag{7}$$

$$\frac{d\lambda_\beta^{\rm ref}}{dt} = \omega_{\rm r}\lambda_\alpha^{\rm ref} - \eta\lambda_\beta^{\rm ref} + \eta L_{\rm m} I_\beta. \tag{8}$$

We first present the development under ideal integration and later discuss the effect of nonideal conditions.

The equations of the single-manifold SM observer are identical to those in (3) and (4). However, the speed estimate is

$$\hat{\omega}_{\rm r} = M \cdot \text{sign}(s). \tag{9}$$

Manifold s is constructed as

$$s = \lambda_\beta^{\rm ref}\hat{\lambda}_\alpha - \lambda_\alpha^{\rm ref}\hat{\lambda}_\beta. \tag{10}$$

The block diagram of the single-manifold SM MRAS method is shown in Fig. 7.

Note that the speed estimate is a discontinuous function of the manifold and M is a positive constant. To show that SM can be enforced in the manifold $s = 0$, we need to show that there

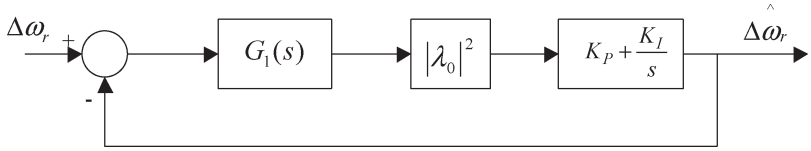

Fig. 2. Speed-estimation dynamics of classical MRAS under ideal integration.

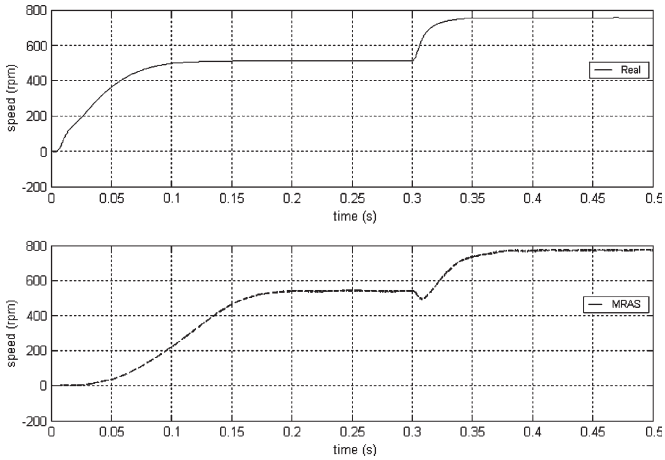

Fig. 3. Real and MRAS estimated speed under nonideal integration.

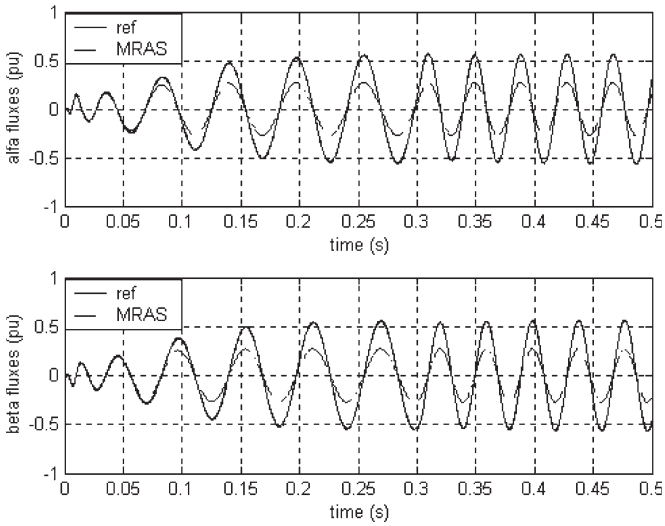

Fig. 4. Real and MRAS estimated fluxes under nonideal integration.

exists M sufficiently high such that the manifold is attractive, i.e., (11) as follows:

$$s \cdot \dot{s} < 0. \tag{11}$$

After differentiating (10) and replacing the derivatives of the fluxes from (3) and (4), and (7) and (8), the following expression is obtained:

$$\dot{s} = f\left(\hat{\lambda}_{\alpha\beta}, \lambda^{\text{ref}}_{\alpha\beta}, \omega_{\text{r}}, \eta, L_{\text{m}}\right) - M\left(\hat{\lambda}_\alpha \lambda^{\text{ref}}_\alpha + \hat{\lambda}_\beta \lambda^{\text{ref}}_\beta\right)\text{sign}(s) \tag{12}$$

where f is a function of the reference and estimate fluxes, speed, and motor parameters. Since the term $(\hat{\lambda}_\alpha \lambda^{\text{ref}}_\alpha + \hat{\lambda}_\beta \lambda^{\text{ref}}_\beta)$ is greater than 0 when the motor is excited and f has a positive upper estimate, it is clear from (12) that sufficiently high M can be selected such that condition (11) is fulfilled. Thus, SM is enforced in the manifold s and after SM begins, we have $s = 0$.

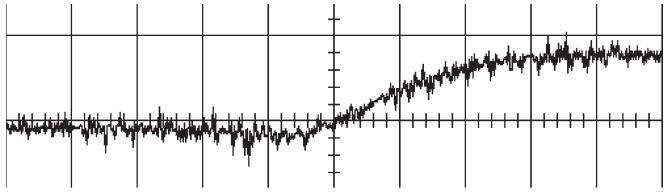

Fig. 5. Estimated speed by classical MRAS under nonideal integration, 225 r/min/div, 1 s/div.

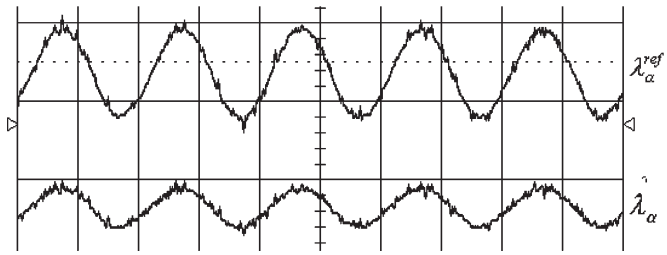

Fig. 6. Reference and observed flux by classical MRAS under nonideal integration, 0.1 Wb/div, 50 ms/div.

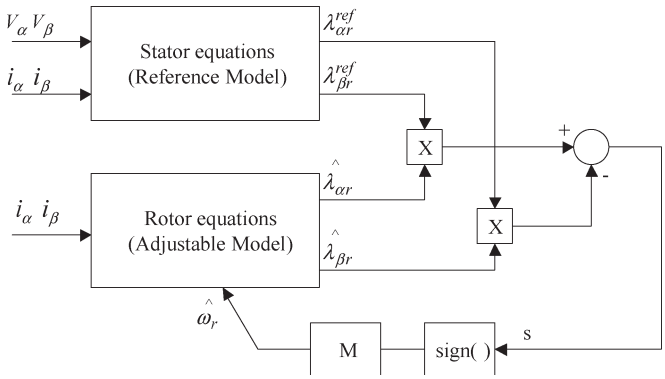

Fig. 7. Block diagram of the single-manifold SM MRAS.

The boundary-layer method described in [9] is used to find the equivalent control $\omega_{\text{r,eq}}$. Once SM occurs, we can also assume $\dot{s} = 0$ along with $s = 0$. The expression of the equivalent control becomes

$$\omega_{\text{r,eq}} = \omega_{\text{r}} + \frac{\eta L_{\text{m}} I_\alpha \left(\lambda^{\text{ref}}_\beta - \hat{\lambda}_\beta\right) + \eta L_{\text{m}} I_\beta \left(\hat{\lambda}_\alpha - \lambda^{\text{ref}}_\alpha\right)}{\left(\hat{\lambda}_\alpha \lambda^{\text{ref}}_\alpha + \hat{\lambda}_\beta \lambda^{\text{ref}}_\beta\right)}. \tag{13}$$

From (13), when the estimated fluxes converge to the reference fluxes, the equivalent speed tends to the real speed. The equivalent speed represents the low-frequency component of

the discontinuous term (9). Thus, while the high-frequency switching function is fed into the observer, its low-frequency component can be obtained by low-pass filtering and represents the speed estimate.

The continuous-time SM concept in [9] is developed under the assumption that the switching frequency of the control is infinite. For implementation with a digital signal processor (DSP), the sampling frequency is finite and the observer equations (3) and (4) must be discretized.

A few choices are available for the switching term (9). With a very small sampling time ($< 50\ \mu$s), expression (14) can be used and the chattering in the flux waveforms will be kept at an acceptable level

$$\hat{\omega}_{\mathrm{r}}(k) = M \cdot \mathrm{sign}(s_k). \tag{14}$$

For larger sampling times, a continuous high-gain approximation of the sign function as in (15) should be used to reduce the discretization chatter (ε is a small positive constant).

$$\hat{\omega}_{\mathrm{r}}(k) = \begin{cases} M \cdot \mathrm{sign}(s_k), & \text{if } |s_k| > \varepsilon \\ \frac{M}{\varepsilon} s_k, & \text{if } |s_k| \le \varepsilon. \end{cases} \tag{15}$$

Compared to (14), (15) is more difficult to implement and requires the tuning of the additional parameter ε. The advantage is that this approach will reduce or may completely eliminate the need for filtering to get the speed estimate.

The proposed observer is simulated in discrete time under the same speed/torque conditions as for the classical MRAS. The approach given by (14) was used. Fig. 8 shows the real and estimated speed under ideal integration; this was obtained through a 15-Hz-bandwidth LPF. For lower ripple, the bandwidth can be reduced. Under ideal integration in the VM observer, the estimated fluxes match the references exactly (not shown).

Figs. 9 and 10 show the behavior under nonideal integration—a 3.18-Hz LPF is used in the VM observer. The waveform of the speed estimate in Fig. 9 has about 10 r/min (2%) error in steady state. However, the dynamics at step change is much improved compared to the classical MRAS. The fluxes estimated by the SM MRAS method differ slightly from the reference fluxes—their amplitude is about 7% bigger. Compared to the flux estimation in Fig. 4, this is a significant improvement.

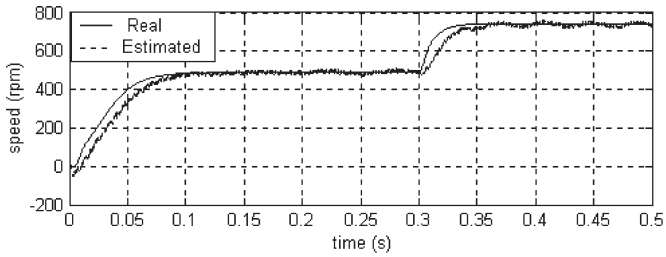

Fig. 8. Real and SM MRAS estimated speed under ideal integration.

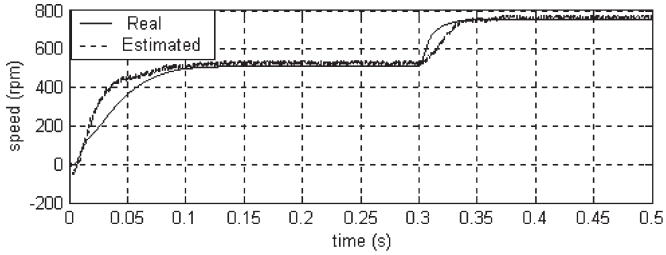

Fig. 9. Real and SM MRAS estimated speed under nonideal integration.

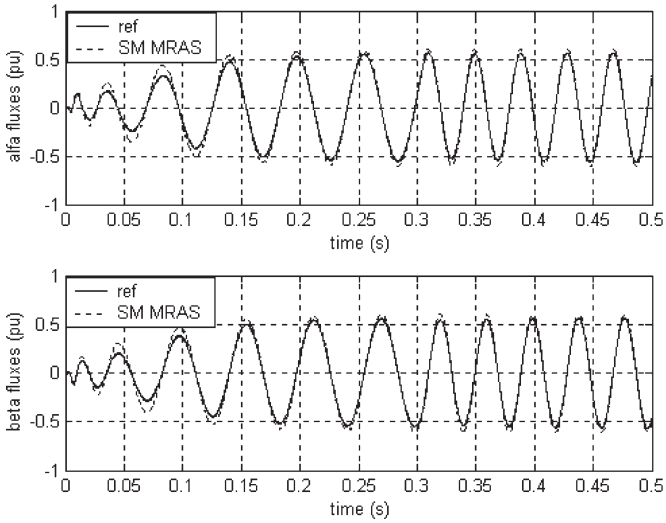

Fig. 10. VM and SM MRAS estimated fluxes under nonideal integration.

IV. MRAS Single-Manifold Discrete-Time SM (DTSM) Observer

The development of the MRAS DTSM observer is based on the theory in [9]. DTSM is defined as the motion of the trajectory of a discrete-time system on a manifold s such that $s(k) = 0$ at sampling times $k = 1, 2, \ldots, n$.

The first design step is to select the system manifold. After that, at sampling time k, the control term $\hat{\omega}_{\mathrm{r}}(k)$ in the observer equations should be computed such that $s(k+1) = 0$. The method is based on the forward (Euler) approximation of the integral to allow computation of the terms in the manifold at sampling time $k+1$. For the observer proposed, the manifold is

$$s(k) = \lambda_{\beta}^{\mathrm{ref}}(k)\hat{\lambda}_{\alpha}(k) - \lambda_{\alpha}^{\mathrm{ref}}(k)\hat{\lambda}_{\beta}(k). \tag{16}$$

The general method cannot be directly applied here because the dynamic system described by (1) and (2) is not in the standard form $\dot{x} = Ax + Bu$, since computation of the rotor fluxes is done by an algebraic equation, not a differential one. The attempt to predictively compute the rotor fluxes for the next sampling time (Euler method) by (2) requires the values of the currents that have not been sampled yet.

To overcome this difficulty, the method has been slightly adapted and will give a speed estimate with a delay of one sampling time. The discrete-time observer equations are

$$\hat{\lambda}_{\alpha,k} = \hat{\lambda}_{\alpha,k-1} + [-\eta\hat{\lambda}_{\alpha,k-1} - \hat{\omega}_{\mathrm{r},k-1}\hat{\lambda}_{\beta,k-1} + \eta L_{\mathrm{m}} I_{\alpha,k-1}]T_{\mathrm{s}} \tag{17}$$

$$\hat{\lambda}_{\beta,k} = \hat{\lambda}_{\beta,k-1} + [\hat{\omega}_{\mathrm{r},k-1}\hat{\lambda}_{\alpha,k-1} - \eta\hat{\lambda}_{\beta,k-1} + \eta L_{\mathrm{m}} I_{\beta,k-1}]T_{\mathrm{s}}. \tag{18}$$

The above right-hand sides and the known quantities $\lambda_{\alpha,k}^{\mathrm{ref}}$ and $\lambda_{\beta,k}^{\mathrm{ref}}$ are inserted in the expression of the manifold (16) and condition $s(k)=0$ is enforced. In this way, the speed estimate $\hat{\omega}_{\mathrm{r},k-1}$ can be computed algebraically. Note that at sampling time k, the method computes a speed estimate for sampling time $k-1$, which is practical since the mechanical speed varies much slower than the electrical variables. The expression obtained is

$$\hat{\omega}_{\mathrm{r},k-1}=\frac{1-\eta T_{\mathrm{s}}}{T_{\mathrm{s}}}\cdot\frac{\lambda_{\beta,k}^{\mathrm{ref}}\hat{\lambda}_{\alpha,k-1}-\hat{\lambda}_{\beta,k-1}\lambda_{\alpha,k}^{\mathrm{ref}}}{\hat{\lambda}_{\alpha,k-1}\lambda_{\alpha,k}^{\mathrm{ref}}+\hat{\lambda}_{\beta,k-1}\lambda_{\beta,k}^{\mathrm{ref}}}+\eta L_{\mathrm{m}}\frac{\lambda_{\beta,k}^{\mathrm{ref}}I_{\alpha,k-1}-\lambda_{\alpha,k}^{\mathrm{ref}}I_{\beta,k-1}}{\hat{\lambda}_{\alpha,k-1}\lambda_{\alpha,k}^{\mathrm{ref}}+\hat{\lambda}_{\beta,k-1}\lambda_{\beta,k}^{\mathrm{ref}}}. \quad (19)$$

Fig. 11 shows the real and estimated speeds by DTSM MRAS under nonideal integration in the reference model. Except for the initial transient when the denominators in (19) rise from zero, the estimate matches the real speed with very small steady-state error and good dynamics.

Fig. 12 shows the reference and DTSM estimated fluxes. After the observer has converged, the error between those is very small. Generally, (19) is relatively complicated and requires a real-time division. As indicated by the discrete equation, the method is not easy to implement, especially with low-cost fixed-point processors. Additionally, it was found by simulation that the first term in (19) is dominant. The term is obtained by multiplying a very large quantity (the term with T_{s} in the denominator) with a very small quantity (the term depending on fluxes). With a fixed-point processor, the digital quantization alone will likely reduce the accuracy of the speed estimate.

V. MRAS Double-Manifold SM Observer

A second MRAS SM observer is proposed under the assumptions that the reference fluxes and motor parameters are known. The observer equations are

$$\frac{d\hat{\lambda}_{\alpha}}{dt}=-U_0\mathrm{sign}(s_{\alpha})+\eta L_{\mathrm{m}}I_{\alpha} \quad (20)$$

$$\frac{d\hat{\lambda}_{\beta}}{dt}=-U_0\mathrm{sign}(s_{\beta})+\eta L_{\mathrm{m}}I_{\beta}. \quad (21)$$

The manifolds are defined as

$$s_{\alpha}=\hat{\lambda}_{\alpha}-\lambda_{\alpha}^{\mathrm{ref}} \quad (22)$$

$$s_{\beta}=\hat{\lambda}_{\beta}-\lambda_{\beta}^{\mathrm{ref}}. \quad (23)$$

Subtracting (7) and (8) from (20) and (21), we obtain

$$\begin{bmatrix}\dot{s}_{\alpha}\\ \dot{s}_{\beta}\end{bmatrix}=\begin{bmatrix}f_{\alpha}\left(\lambda_{\alpha}^{\mathrm{ref}},\lambda_{\beta}^{\mathrm{ref}},\eta,\omega_{\mathrm{r}}\right)\\ f_{\beta}\left(\lambda_{\alpha}^{\mathrm{ref}},\lambda_{\beta}^{\mathrm{ref}},\eta,\omega_{\mathrm{r}}\right)\end{bmatrix}-U_0\begin{bmatrix}1&0\\0&1\end{bmatrix}\cdot\begin{bmatrix}\mathrm{sign}(s_{\alpha})\\ \mathrm{sign}(s_{\beta})\end{bmatrix}. \quad (24)$$

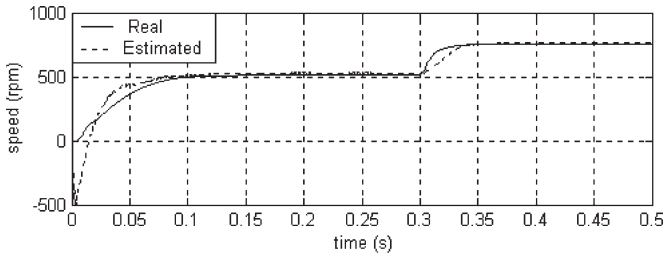

Fig. 11. Real and DTSM MRAS estimated speed under nonideal integration.

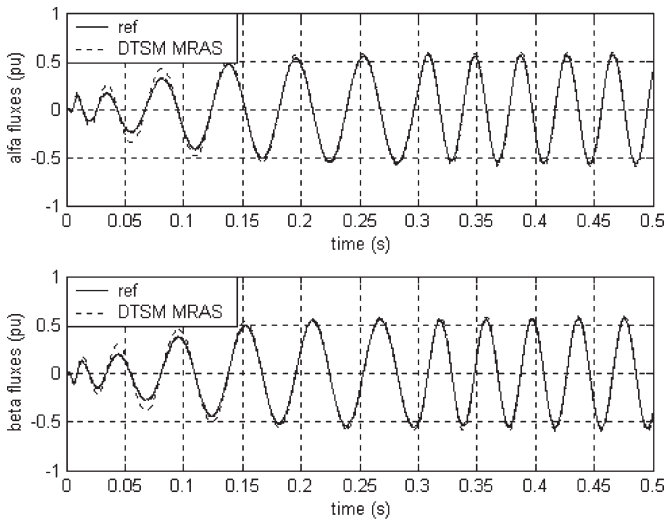

Fig. 12. Real and DTSM MRAS estimated speed under nonideal integration.

Since f_{α} and f_{β} both have positive upper estimates and the identity matrix is positive definite, (24) satisfies the sufficient condition for SM to exist as it was formulated in [9]. Consequently, the positive constant U_0 can be selected high enough such that SM is enforced on the intersection of the two manifolds. After SM occurs, $s_{\alpha}=0$, $s_{\beta}=0$ identically, and the observed fluxes equal the reference fluxes.

If the switching functions s_{α} and s_{β} are filtered, the equivalent controls are obtained. We will denote the equivalent controls as $\Psi_{\alpha}^{\mathrm{eq}}$ and $\Psi_{\beta}^{\mathrm{eq}}$, representing the low-frequency components of the switching functions. Comparison of the original (7) and (8) to the observer equations yields the following result:

$$\begin{bmatrix}\Psi_{\alpha}^{\mathrm{eq}}\\ \Psi_{\beta}^{\mathrm{eq}}\end{bmatrix}=\begin{bmatrix}-\lambda_{\alpha}^{\mathrm{ref}}&-\lambda_{\beta}^{\mathrm{ref}}\\ -\lambda_{\beta}^{\mathrm{ref}}&\lambda_{\alpha}^{\mathrm{ref}}\end{bmatrix}\cdot\begin{bmatrix}\eta\\ \omega_{\mathrm{r}}\end{bmatrix}=\Lambda\cdot\begin{bmatrix}\eta\\ \omega_{\mathrm{r}}\end{bmatrix}. \quad (25)$$

If the motor is excited, matrix Λ is nonsingular $(\det(\Lambda)=-(\lambda_{\alpha}^{\mathrm{ref}^2}+\lambda_{\beta}^{\mathrm{ref}^2})\neq 0)$. Therefore, system (25) has a unique solution and the rotor speed estimate is

$$\omega_{\mathrm{r}}=\frac{\lambda_{\alpha}^{\mathrm{ref}}\psi_{\beta}^{\mathrm{eq}}-\lambda_{\beta}^{\mathrm{ref}}\Psi_{\alpha}^{\mathrm{eq}}}{\lambda_{\alpha}^{\mathrm{ref}^2}+\lambda_{\beta}^{\mathrm{ref}^2}}. \quad (26)$$

The equivalent controls are needed to compute the speed estimate—these are sinusoidal signals of the stator frequency. Unlike the single-manifold SM observer (where the LPF bandwidth was only influencing the output ripple), here, the LPF does not only attenuate the high frequencies but also affects the

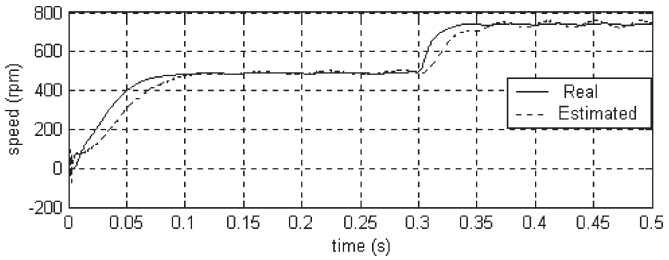

Fig. 13. Real and estimated speed by two-dimensional SM MRAS under nonideal integration.

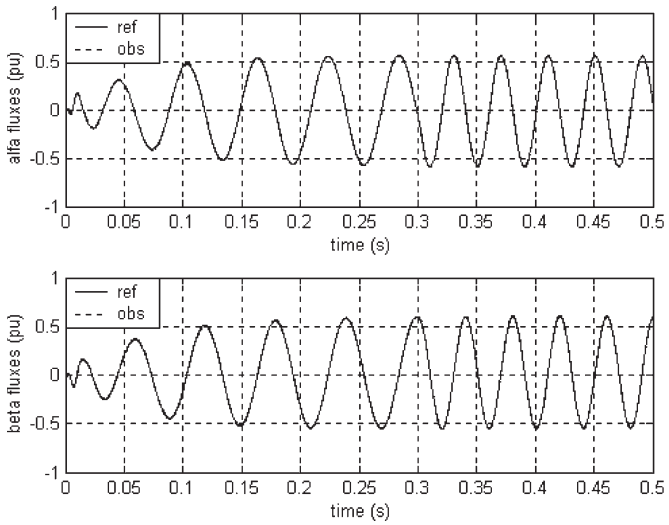

Fig. 14. Reference and estimated fluxes by two-dimensional SM MRAS under nonideal integration.

magnitude/phase of the low-frequency sinusoidal signal. This makes the selection of the LPF time constant more difficult. If the stator frequency increases towards the LPF bandwidth, the attenuation of $\Psi_\alpha^{\rm eq}$ and $\Psi_\beta^{\rm eq}$ is significant and will produce errors in (26). On the other hand, if a high bandwidth is chosen, little filtering is achieved at low frequency. To avoid this problem, the switching manifolds are designed using (15). Thus, the SM gains are reduced as the observer trajectories approach the manifolds. Simulation shows that no filtering is needed. Fig. 13 shows the simulated speed estimate in the same speed/torque conditions as before and with nonideal integration in the reference model.

Fig. 14 shows the reference and estimated fluxes, displaying a very good agreement.

The waveforms of the two equivalent controls used for computations are shown in Fig. 15, indicating no need to filter them. When the speed increases at $t = 0.3$ s, their magnitude also increases, as it was expected from (26).

Note that system (25) contains a second equation and this may offer the illusion that the inverse of the rotor time constant η can also be estimated along with the rotor speed. Unfortunately, this is not true. Equation (25) is valid if and only if η used in the observer equations (20) and (21) is equal to the real value. Our simulation study confirms that under incorrect η, the speed estimate has steady-state error. For example, if the rotor resistance increases by 50% and the SM observer runs with the

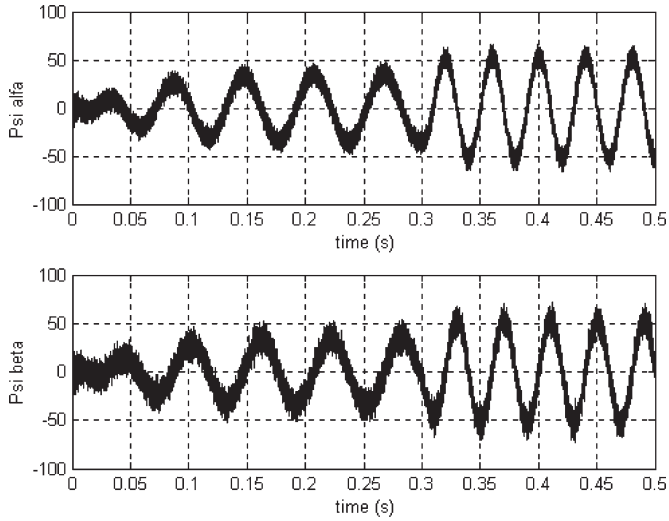

Fig. 15. Equivalent controls $\Psi_\alpha^{\rm eq}$ and $\Psi_\beta^{\rm eq}$, in webers per second.

TABLE I
MOTOR SPECIFICATIONS AND PARAMETERS

Rating	*¼hp*	Pole #	4
Speed	*1732 rpm*	Voltage	220 V
R_s		10.9 Ω	
L_{ls},L_{lr}		0.015 H	
L_m		0.30 H	
Rr		5.57 Ω	

rated value, the error at small load (0.2-pu torque) is about 10% and is as high as 60% at high load (1-pu torque).

VI. EXPERIMENTAL RESULTS

The induction motor used in the experimental testing is a typical three-phase squirrel-cage machine. The specifications and parameters are listed in Table I.

The motor is powered by an insulated gate bipolar transistor (IGBT) inverter. The DSP for controller implementation is a 16-bit fixed-point TMS320-F2407PGEA with four D/A channels used to output the waveforms of interest. The controller software is organized in two interrupts. A fast interrupt (50 μs) processes the feedback signals, and runs the classical VM observer and the SM observer. The VM-produced fluxes are used for direct field orientation control of the motor. A slow interrupt (115 μs) regulates the rotor speed and outputs the PWM commands. The inverter switching frequency is at 8.7 kHz. The phase currents are measured through two Hall sensors. Stator voltages are computed using the switching states of the inverter. Since our setup does not have a speed sensor, the SM speed estimates are compared with the estimates given by the slip method (27) (also called classic method)

$$\omega_{\rm r} = \omega_{\rm s} - \omega_{\rm slip}. \tag{27}$$

Fig. 16 shows the reference and observed fluxes by the single-manifold SM MRAS at a rotor speed of approximately 250 r/min and no load. The flux waveforms are very similar to each other in both magnitude and phase.

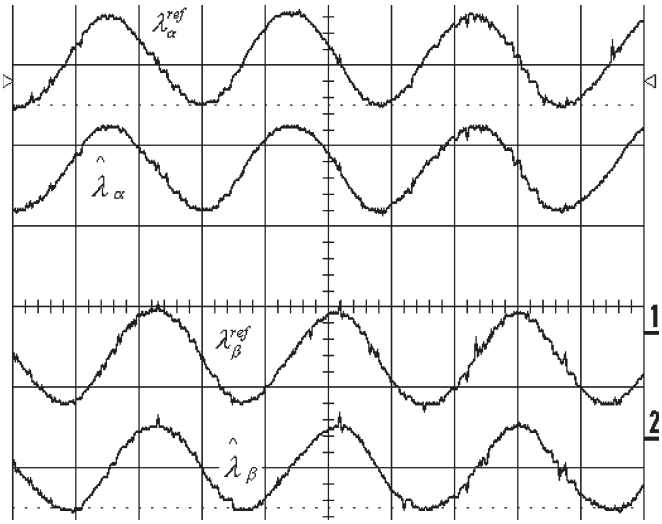

Fig. 16. Single-manifold SM MRAS, 0.1 Wb/div, 20 ms/div.

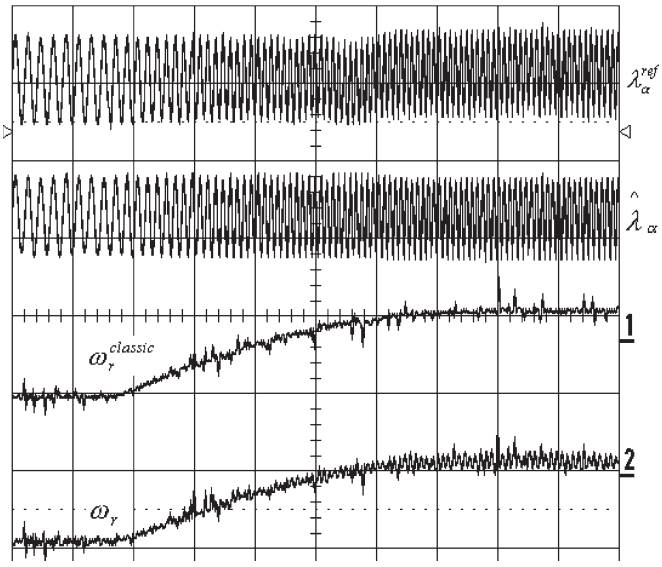

Fig. 17. Single-manifold SM MRAS, 0.1 Wb/div, 225 r/min/div, 500 ms/div.

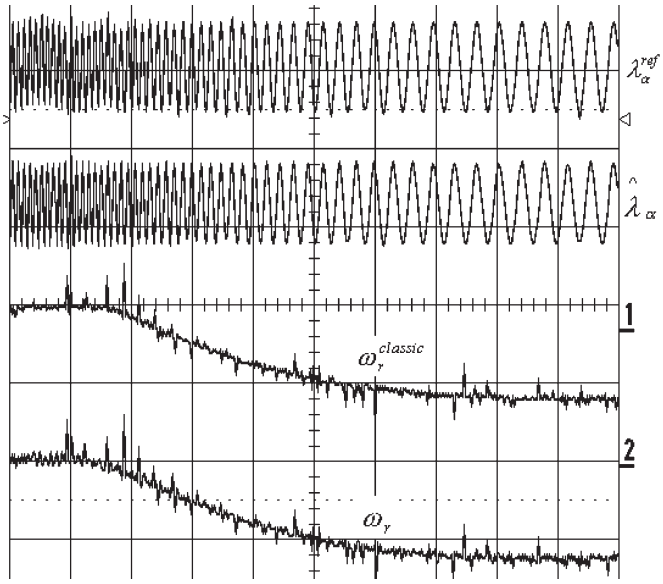

Fig. 18. Single-manifold SM MRAS, 0.1 Wb/div, 225 r/min/div, 500 ms/div.

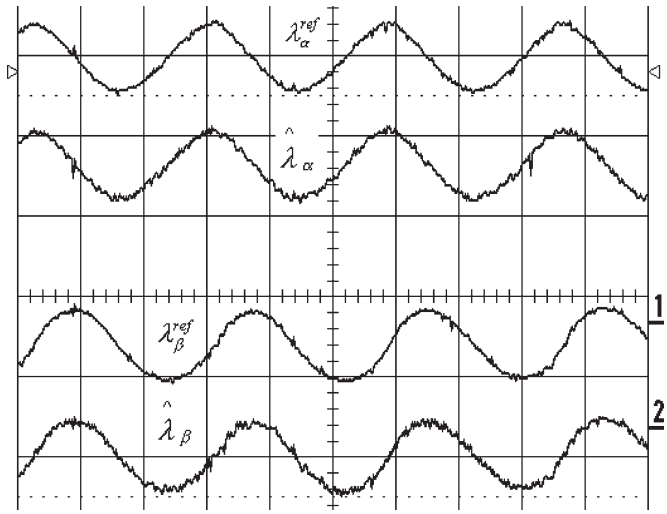

Fig. 19. Double-manifold SM MRAS, 0.1 Wb/div, 20 ms/div.

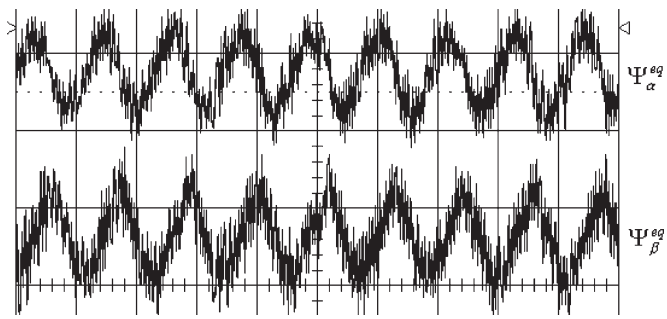

Fig. 20. Double-manifold SM MRAS, 50 Wb/s/div, 50 ms/div.

The α reference flux, the observed flux of the single-manifold SM MRAS, and the speed estimated by (27) and by the proposed method are shown in Fig. 17 (100–350-r/min acceleration) and Fig. 18 (350–100-r/min deceleration), respectively. It can be seen that the speed dynamics has no dip or underdamped behavior and the magnitudes of the estimates are quite close. Fig. 19 shows the fluxes of the double-manifold SM MRAS. In this case, the selection of the manifolds guarantees that the estimated fluxes match the references.

Equivalent controls Ψ_α^{eq} and Ψ_β^{eq} are shown in Fig. 20.

Fig. 21 shows the fluxes and speed estimates for a 100–350-r/min acceleration. Experimentally, it was found that both methods are very robust to disturbances. For the single-manifold method, the SM gains and the time constant of the LPF are easy to tune and the method is quite accurate. For the double-manifold observer, the additional design parameter ε needs to be selected and it must be checked that the reduction of the SM gain in (15) takes place.

For a fixed-point processor, the latter method is more computationally intensive, especially due to the real-time division in (26). Also, for very accurate estimation, it seems that a DSP with 32×16 bit multiplications will help.

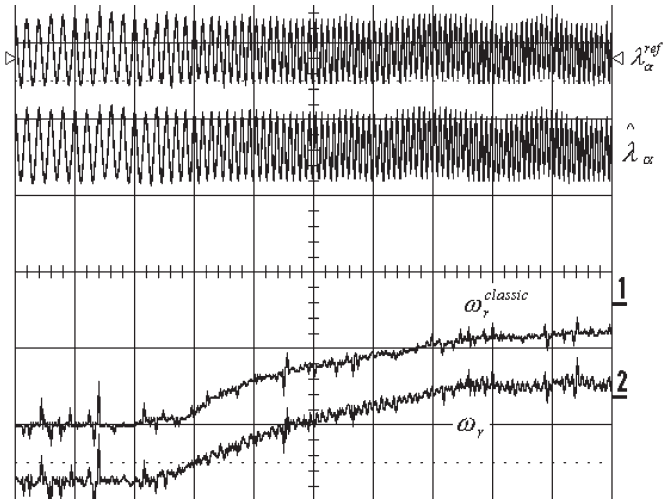

Fig. 21. Double-manifold SM MRAS, 0.1 Wb/div, 225 r/min/div, 500 ms/div.

VII. Conclusion

This paper discusses some of the problems associated with the classical flux MRAS method under nonideal integration and proposes two novel SM MRAS speed estimators. The speed estimate is to be used in the feedback loop of a sensorless induction motor drive. The methods proposed are relatively easy to implement and only require the appropriate selection of the SM gains. Unlike the classical MRAS, in the proposed methods, the speed is estimated by either low-pass filtering or by algebraic equations. The dynamics of the speed estimate obtained by the SM technique does not exhibit damped responses or speed dip caused by right-hand-plane zeros. Simulations and experiments prove that good accuracy and improved dynamics are obtained, even on a low-cost DSP.

References

[1] B. K. Bose, *Modern Power Electronics and AC Drives*. Upper Saddle River, NJ: Prentice-Hall, 2002.

[2] C. Schauder, "Adaptive speed identification for vector control of induction motors without rotational transducers," *IEEE Trans. Ind. Appl.*, vol. 28, no. 5, pp. 1054–1061, Sep./Oct. 1992.

[3] H. Tajima and Y. Hori, "Speed sensorless field orientation control of induction machine," *IEEE Trans. Ind. Appl.*, vol. 29, no. 1, pp. 175–180, Jan./Feb. 1993.

[4] R. Blasco-Gimenez, G. M. Asher, M. Sumner, and K. J. Bradley, "Dynamic performance limitations for MRAS based sensorless induction motor drives. Part 1: Stability analysis of the closed loop drive," *Proc. Inst. Elect. Eng.—Electr. Power Appl.*, vol. 143, no. 2, pp. 113–122, Mar. 1996.

[5] M. N. Marwali and A. Keyhani, "A comparative study of rotor flux based MRAS and back EMF based MRAS speed estimators for speed sensorless vector control of induction machines," in *Conf. Rec. IEEE-IAS Annu. Meeting*, New Orleans, LA, Oct. 5–9, 1997, pp. 160–166.

[6] F. Z. Peng and T. Fukao, "Robust speed identification for speed-sensorless vector control of induction motors," *IEEE Trans. Ind. Appl.*, vol. 30, no. 5, pp. 1234–1240, Sep./Oct. 1994.

[7] J. Holtz and J. Quan, "Drift and parameter compensated flux estimator for persistent zero stator frequency operation of sensorless controlled induction motors," *IEEE Trans. Ind. Appl.*, vol. 39, no. 4, pp. 1052–1060, Jul./Aug. 2003.

[8] J. Hu and B. Wu, "New integration algorithms for estimating motor flux over a wide speed range," *IEEE Trans. Power Electron.*, vol. 13, no. 5, pp. 969–977, Sep. 1998.

[9] V. I. Utkin, J. G. Guldner, and J. Shi, *Sliding Mode Control in Electromechanical Systems*. New York: Taylor & Francis, 1999.

Mihai Comanescu (S'02) was born in Bucharest, Romania, in 1968. He received the B.S.E.E. degree from the Bucharest Polytechnic Institute, Bucharest, Romania, in 1992, and the M.S. and Ph.D. degrees in electrical engineering from The Ohio State University, Columbus, in 2001 and 2005, respectively.

He is currently with Azure Dynamics, Woburn, MA, working on electric vehicle development. His research interests are in the areas of power electronics, ac drives, and motion control systems.

Longya Xu (S'89–M'90–SM'93–F'04) received the M.S. and Ph.D. degrees from the University of Wisconsin, Madison, in 1986 and 1990, respectively, all in electrical engineering.

He joined the Department of Electrical and Computer Engineering at The Ohio State University, Columbus, in 1990, where he is currently a Professor. He has served as a Consultant to many industry companies including Raytheon Company, U.S. Wind Power Company, General Motors, Ford, and Unique Mobility Inc. for various industrial concerns. His research and teaching interests include dynamic modeling and optimized design of electrical machines and power converters for variable speed generation and drive systems, application of advanced control theory, and digital signal processor for motion control and distributed power systems in super-high-speed operation.

Dr. Xu received the 1990 First Prize Paper Award from the Industrial Drives Committee, IEEE Industry Applications Society (IAS). In 1991, he won a Research Initiation Award from the National Science Foundation. He is also a recipient of the 1995 and 1999 Lumley Research Awards for his outstanding research accomplishments from the College of Engineering, The Ohio State University. He has served as the Chairman of the Electric Machine Committee of the IAS and an Associate Editor of IEEE Transactions on Power Electronics.